RESEARCH ARTICLE

Macromolecular Rapid Communications
www.mrc-journal.de

Functional Mesostructured Electrospun Polymer Nonwovens with Supramolecular Nanofibers

Andreas Frank, Melina Weber, Christian Hils, Ulrich Mansfeld, Klaus Kreger, Holger Schmalz, and Hans-Werner Schmidt**

Functional, hierarchically mesostructured nonwovens are of fundamental importance because complex fiber morphologies increase the active surface area and functionality allowing for the effective immobilization of metal nanoparticles. Such complex functional fiber morphologies clearly widen the property profile and enable the preparation of more efficient and selective filter media. Here, the realization of hierarchically mesostructured nonwovens with barbed wire-like morphology is demonstrated by combining electrospun polystyrene fibers, decorated with patchy worm-like micelles, with solution-processed supramolecular short fibers composed of 1,3,5-benzenetricarboxamides with peripheral *N*,*N*-diisopropylaminoethyl substituents. The worm-like micelles with a patchy microphase-separated corona are prepared by crystallization-driven self-assembly of a polyethylene based triblock terpolymer and deposited on top of the polystyrene fibers by coaxial electrospinning. The micelles are designed in a way that their patches promote the directed self-assembly of the 1,3,5-benzenetricarboxamide and the fixation of the supramolecular nanofibers on the supporting polystyrene fibers. Functionality of the mesostructured nonwoven is provided by the peripheral *N*,*N*-diisopropylaminoethyl substituents of the 1,3,5-benzenetricarboxamide and proven by the effective immobilization of individual palladium nanoparticles on the supramolecular nanofibers. The preparation of hierarchically mesostructured nonwovens and their shown functionality demonstrate that such systems are attractive candidates to be used for example in filtration, selective separation and heterogenous catalysis.

1. Introduction

Multifunctional hierarchical and mesostructured fibrous materials are expected to play a key role for the preparation of a new generation of filter media and membranes in life science and materials science. This includes for example personal protective equipment such as face masks with improved moisture permeability, antiviral and antibacterial properties as well as fibrous membranes with self-sustained long-range electrostatic adhesion for energy generation and compact composite sheets for catalysis.[1–4]

Conventional polymer micro- and nanofibers are achieved by top-down methods such as melt blowing,[5] centrifugal spinning,[6–8] and electrospinning.[9–11] These spinning processes are well-established and typically allows to create free-standing nonwovens or nonwovens deposited on top of a support. Improvement in this field is expected to fabricate nonwovens with different hierarchical levels in the fiber morphology.[12,13] Consequently, hierarchy is described by the combination of two or more fiber types with different fiber diameters of the entire nonwoven. This may also result in hierarchal levels

A. Frank, M. Weber, K. Kreger, H.-W. Schmidt
Macromolecular Chemistry I and Bavarian Polymer Institute (BPI)
University of Bayreuth
Universitätsstraße 30, Bayreuth 95447, Germany
E-mail: hans-werner.schmidt@uni-bayreuth.de

C. Hils, H. Schmalz
Macromolecular Chemistry II and Bavarian Polymer Institute (BPI)
University of Bayreuth
Universitätsstraße 30, Bayreuth 95447, Germany
E-mail: holger.schmalz@uni-bayreuth.de

U. Mansfeld
Bavarian Polymer Institute (BPI)
University of Bayreuth
Universitätsstraße 30, Bayreuth 95447, Germany

The ORCID identification number(s) for the author(s) of this article can be found under https://doi.org/10.1002/marc.202200052

Dedicated to Professor Rudolf Zentel

DOI: 10.1002/marc.202200052

with respect to the pore size distribution. For example, Zhang et al. prepared composites with different fiber diameters and pore sizes via sequential or multijet electrospinning of different polymers which shows improved filtration efficiency.[14,15] Another example of a hierarchical double layer structured composite was described by Wang et al. consisting of micro- and nanosized porous fibers and nanosized fibers of polylactic acid.[16]

Furthermore, Su et al. reviewed the combination of polymer fibers with carbon nanotubes (CNTs), demonstrating that CNTs are important for reinforcement and enhanced properties like mechanical strength and electrical conductivity.[17]

Another promising approach to achieve composites with different hierarchical fiber levels is the combination of polymer fibers and supramolecular fibers. In general, the preparation of supramolecular fibers is realized by self-assembly of molecular building blocks via directed secondary interactions. The unique feature of such a bottom-up approach is the in situ formation of the supramolecular fibers from solution, which enables the realization of composite fibers in an existing scaffold. In this context, we have demonstrated the preparation of microfiber/nanofiber composites using a commercial viscose polyester-based microfiber nonwoven and selected 1,3,5-benzenetricaboxamides (BTAs) as building blocks. These composites were found to be highly suitable for air filtration applications.[18,19] Hu et al. and Wang et al. have shown that selected small molecular sorbitol derivates enable the formation of supramolecular nanofiber webs within solution-blown polyacrylonitrile (PAN) nanofibers.[2,20] Such fiber composites can be used as air filter media with an improved moisture permeation due to the loading with the hydrophilic sorbitol nanofibers.[2]

Apart from these hierarchical supramolecular/polymer fiber composites, we have recently reported on mesoscale nonwovens, in those the supramolecular nanofibers feature a dedicated functionality enabling the efficient immobilization of gold nanoparticles. For this, we employed the wet-laid technique using a mixture of short electrospun PAN and supramolecular nanofibers based on BTAs with functional terpyridine side groups in the periphery resulting in compact functional nonwoven sheets.[4]

Besides these kinds of nonwovens, whose morphologies are a result of the combination of different fiber types, nature uses an intriguing approach based on hierarchically mesostructured fibers as present in plants like thistles and animal feathers. Such hierarchically mesostructured fibers comprise a middle strand with off-standing thinner branches and feature a superior property profile. In this context, we have demonstrated the preparation of hierarchically mesostructured nonwovens comprising an electrospun supporting polymer fiber with off-standing branches of nonfunctional supramolecular BTA fibers. Consequently, the hierarchical level refers to a fibrous superstructure, which we refer here as hierarchical mesostructured fibers. This morphology was realized by depositing BTA seeds on the electrospun fibers followed by an in situ growth of the BTA nanofibers from solution leading to a penguin downy feather-like morphology.[21] Such nonwovens enable the removal of particulate matter from air with improved efficiency while at the same time a low pressure drop is maintained.[21]

In a proof-of-concept we have also realized hierarchical superstructures composed of electrospun patchy polymer fibers with off-standing functional supramolecular fibers, utilizing a combination of crystallization-driven self-assembly (CDSA)[22–25] and molecular self-assembly.[26] The patchy polymer fibers consist of supporting polystyrene (PS) fibers that were decorated with patchy worm-like micelles (prepared by CDSA) via coaxial electrospinning. The functional patches on the polymer fiber's surface locally increase the BTA concentration driven by the chemical match of the peripheral amino groups of the BTA with the respective amino groups in the surface patches. This in turn promotes the patch-mediated molecular self-assembly of the BTA from the polymer fiber surface, resulting in a fir-tree like superstructure.[26]

Here, we report on hierarchically mesostructured nonwovens with a barbed wire-like morphology combining electrospun PS fibers, decorated with patchy worm-like micelles, and supramolecular nanofibers based on BTAs with functional tertiary amino substituents (**Figure 1**). The molecular self-assembly process is induced by a local enrichment of the BTA close to the patches due to the chemical similarity of one block of the patches and the periphery of the molecular building block. The chemical similarity between both also promotes the fixation of the supramolecular nanofibers on the supporting PS fiber. These hierarchical mesostructured fibers can be regarded as a fibrous superstructure, where in particular the off-standing branches feature an additional functionality. Here, the amino functionality in the periphery of the BTA can be harnessed for the immobilization of metal nanoparticles on the surface of the supramolecular nanofibers.

2. Results and Discussion

2.1. Solubility and Self-Assembly Behavior of the Functional 1,3,5-Benzenetricarboxamide

An important aspect of our functional, hierarchically mesostructured nonwovens is the preparation of supramolecular nanofibers with a high surface to volume area and a high functionality on the fibers' surface. Ready access to the functional groups of the supramolecular fibers allows for an effective immobilization of metal nanoparticles from aqueous media. As supramolecular motif for the structure formation, we focused on the well-known material class of BTAs. Under proper conditions, BTAs are known to self-assemble into fibrous nano-objects with a columnar structure created by the formation of three directed hydrogen bonds.[27] Functionality was introduced in the periphery using *N*,*N*-diisopropylaminoethyl substituents. These groups were selected since block copolymers featuring tertiary amino side groups were demonstrated to efficiently immobilize metal nanoparticles.[28–32] In contrast to BTAs with *N*,*N*-dimethylaminoethyl or *N*,*N*-diethylaminoethyl side groups,[33] BTAs with bulkier tertiary amino groups are not water-soluble. Thus, their structures are expected to be stable in aqueous media without disintegration. A similar behavior in view of water solubility was found for poly(*N*,*N*-dialkylaminoethyl methacrylamides) and poly(*N*,*N*-dialkylaminoethyl methacrylates) with pendant tertiary amino groups, i.e., water solubility decreases with increasing length of the alkyl substituents at the amino group.[34–36] For this purpose, N^1,N^3,N^5-tris[2-(diisopropylamino)-ethyl]-1,3,5-benzenetricarboxamide (*i*Pr-BTA, see **Figure 2**A inset) was

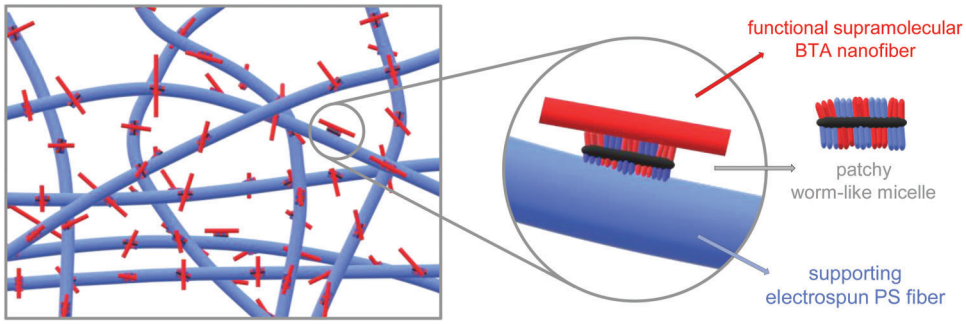

Figure 1. Schematic representation of a section of the hierarchically mesostructured electrospun PS nonwoven (blue) with functional supramolecular BTA nanofibers (red), with the magnification on the right showing the individual components. The mesostructured nonwoven comprises electrospun PS fibers as support with deposited patchy worm-like micelles on their surface. The patchy micelles promote the BTA self-assembly due to the chemical similarity of the patches, which results in a local enrichment of the BTA building blocks, as well as the fixation of the BTA nanofibers on the supporting electrospun PS fibers.

synthesized in a similar manner as described previously.[33] Detailed information on the synthesis and molecular characterization is given in the Experimental Section. Fourier transformation infrared (FT-IR) spectroscopy was used to provide evidence for the formation of strong hydrogen bonds of *i*Pr-BTA in bulk. In particular the N–H stretch vibrations at $\tilde{\upsilon} = 3240$ cm^{-1} and the N–H bend and C–N stretch vibrations at $\tilde{\upsilon} = 1560$ cm^{-1} indicate a columnar stacking[37] (Figure S1, Supporting Information) and is expected to promote nanofiber formation. This also indicates that the surfaces of supramolecular columns consist of densely packed functional tertiary amino groups.

Prior to the nanofiber formation, we have investigated the solubility behavior of *i*Pr-BTA. Indeed, we found that *i*Pr-BTA features a solubility of less than 0.001 wt% in water at room temperature and at elevated temperatures. In contrast, polar organic solvents such as alcohols and in particular isopropanol were identified as suitable solvents. In general, alcohols allow the preparation of clear solutions with *i*Pr-BTA concentrations up to $c \approx 4.00$ wt% at elevated temperatures. To get a more detailed picture, we have performed temperature-dependent solubility and self-assembly studies of *i*Pr-BTA in isopropanol in the concentration range from $c = 0.25$ to 4.25 wt%. Initially, *i*Pr-BTA was dispersed in isopropanol at room temperature. With the exception of concentrations above $c = 4.00$ wt%, *i*Pr-BTA can be molecularly dissolved at 70 °C. Theses samples were subsequently used to determine the temperature-dependent transmittance and, thus, the cloud and clearing points upon cooling and heating in the range of −5 and 70 °C at a rate of 0.1 K min^{-1}. Cloud and clearing points were determined at 50% of transmittance. Exemplarily, the temperature-dependent transmittance upon cooling and subsequent heating of the sample with a concentration of $c = 2.75$ wt% is shown in Figure 2A. Upon cooling, a rapid change in transmittance from 100% to 0% is observed resulting in clouding of the solution and the cloud point ($T_{\text{cloud point}}$) was determined to 55 °C. This process is fully reversible upon heating as it can be observed again by a rapid change in transmittance from 0% to 100%. The clearing point ($T_{\text{clearing point}}$) was found to be 60 °C, reflecting a small hysteresis of about 5 °C between the cloud and clearing point.

Based on all cloud and clearing points, we established a phase diagram of *i*Pr-BTA in isopropanol from 0 to 70 °C as shown in Figure 2B. Three regimes can be identified: up to a concentration of $c = 0.50$ wt%, the *i*Pr-BTA is completely soluble in the investigated temperature range (regime I). Fully reversible self-assembly behavior was observed in the concentration range of $c = 0.75 - 4.00$ wt% (regime II), followed by regime III, in which *i*Pr-BTA cannot be completely dissolved anymore at elevated temperatures. In regime II, with increasing concentration of the *i*Pr-BTA, the cloud points increase from 10 to 63 °C and the clearing points from 27 to 68 °C. At higher concentrations of more than 3.00 wt%, the cloud and clearing points seem to level off. This process is highly reproducible as indicated by the small error bars of the mean values for the cloud and clearing temperatures in Figure 2B. Upon cooling below the respective cloud point, the solution forms a turbid gel as exemplarily shown for a sample containing $c = 2.00$ wt% of the *i*Pr-BTA as depicted in the inset of Figure 2B. The presence of thermo-reversible organogels based on BTAs is very often indicative for the formation of supramolecular (nano)fibers.[38–41] Thus, we have selected the 2.00 wt% gel sample, removed the solvent at ambient conditions and investigated the morphology by scanning electron microscopy (SEM). The SEM image revealed a dense network of supramolecular nanofibers as well as larger bundled aggregates of those. After evaluating the diameter of ≈50 individual supramolecular nanofibers, we found a mean fiber diameter of around 320 ± 130 nm (Figure 2C).

2.2. Preparation of Hierarchically Mesostructured Nonwovens

Following our concept described in Figure 1, hierarchically mesostructured nonwovens were prepared employing a PS nonwoven decorated with patchy worm-like micelles for the directed molecular self-assembly of *i*Pr-BTA nanofibers from the nonwovens' surface. The patchy nonwoven was produced by coaxial electrospinning, using a PS solution as the core and a dispersion of patchy worm-like micelles based on a polystyrene-*block*-polyethylene-*block*-poly(*N*,*N*-diisopropylaminoethyl methacrylamide) (SED*i*PA) triblock terpolymer as shell (Figure S2, Supporting Information), similar to the procedure described previously.[26,30] Accordingly, the nonwovens will be termed patchy PS$_{\text{core}}$/SED*i*PA nonwovens in the following. The patchy, worm-like SED*i*PA micelles (average length: 260 ± 100 nm)

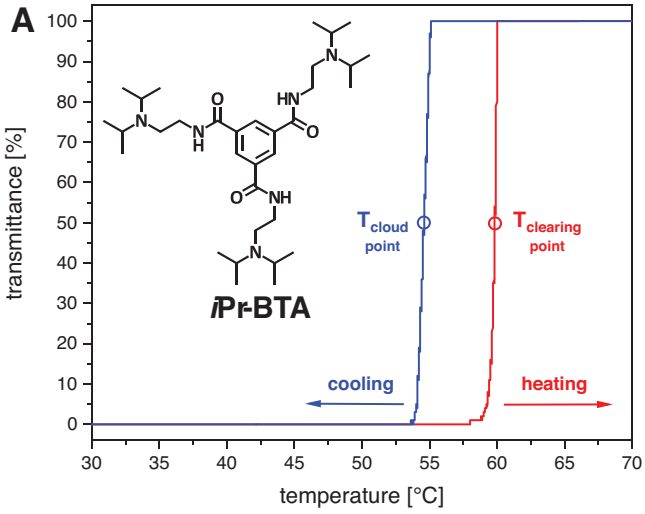

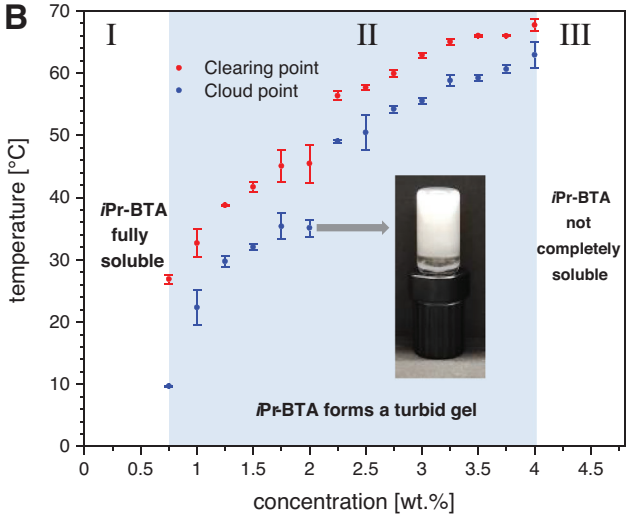

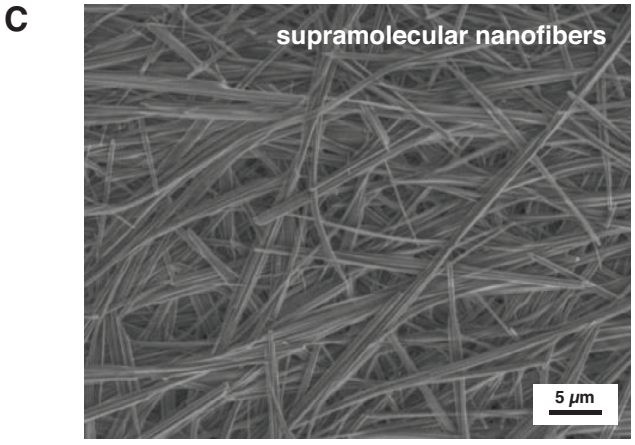

Figure 2. Self-assembly behavior of N^1,N^3,N^5-tris[2-(diisopropylamino)-ethyl]-1,3,5-benzenetricarboxamide (*i*Pr-BTA). A) Temperature-dependent transmittance of *i*Pr-BTA in isopropanol at a concentration of $c = 2.75$ wt% at a heating/cooling rate of 0.1 K min^{-1}. Upon cooling the *i*Pr-BTA solution, clouding of the sample occurs at $T_{cloud\ point} = 55$ °C and a gel is obtained. Upon heating, the gel dissolves again at $T_{clearing\ point} = 60$ °C resulting in a clear solution. This process is fully reversible. B) Concentration-dependent evolution of the cloud and clearing points of *i*Pr-BTA in isopropanol. Indicated are three regimes (I-III). At low concentrations, the *i*Pr-BTA remains dissolved in the investigated temperature range (regime I). With increasing concentration, the *i*Pr-BTA forms a gel upon cooling and fully dissolves upon heating (regime II). At very high concentrations *i*Pr-BTA is not completely soluble (regime III). C) SEM micrograph of a dried gel from a 2.00 wt% solution of *i*Pr-BTA showing long uniform supramolecular nanofibers with a diameter of around 320 nm of the single fibers.

were prepared by CDSA in THF and are composed of a semi-crystalline polyethylene core and a patch-like microphase-separated corona with nanometer-sized PS (12 ± 2 nm) and poly(*N*,*N*-diisopropylaminoethyl methacrylamide) (PD*i*PA; 10 ± 3 nm) patches in the corona (Figure S3, Supporting Information).[30,42] Here, the PS patches guarantee a good adhesion to the supporting PS nonwoven and the PD*i*PA patches bear pendant *N*,*N*-diisopropylaminoethyl groups matching the peripheral groups of *i*Pr-BTA. We note, that the well-defined nanophase-separated patchy worm-like micelles are essential to promote the local increase of the *i*Pr-BTA concentration close to the patches and thus the molecular self-assembly of *i*Pr-BTA. Coating the supporting PS fiber with the corresponding di- or triblock copolymer do not lead to the formation of defined superstructures demonstrating the beneficial role of the patchy micelles prepared by CDSA.

Details on the coaxial electrospinning process, molecular characteristics of SED*i*PA and employed CDSA conditions can be found in the Experimental Section.

For the directed molecular self-assembly of *i*Pr-BTA from the surface of the patchy nonwoven, isopropanol solutions with concentrations at which *i*Pr-BTA is molecularly dissolved at elevated temperatures as well as at room temperature were selected. This ensures that molecular self-assembly of *i*Pr-BTA does not take place prior to solvent evaporation and consequently allows solution uptake within the entire patchy PS$_{core}$/SED*i*PA nonwoven. Therefore, solutions within regime I (see Figure 2B) were chosen with concentrations up to $c = 0.50$ wt% of *i*Pr-BTA in isopropanol. Under these conditions, supramolecular nanofiber formation can only be initiated by solvent evaporation leading to an increase in concentration and consequently self-assembly after reaching a threshold concentration (Figure S4, Supporting Information).

To validate the molecular self-assembly of *i*Pr-BTA from solution initiated close to the patches on the polymer fibers, we have separately deposited patchy PS$_{core}$/SED*i*PA fibers as well as neat electrospun PS fibers as reference on aluminum foil and subsequently immersed both samples in a solution of 0.10 wt% *i*Pr-BTA in isopropanol. SEM images of the neat PS and the patchy PS$_{core}$/SED*i*PA fibers before the immersion are shown in Figure S5A,B in the Supporting Information. On the surface of the patchy PS$_{core}$/SED*i*PA fiber the worm-like micelles can be clearly recognized. After immersion and solvent evaporation at ambient conditions, the resulting morphologies were investigated by SEM. No supramolecular *i*Pr-BTA fibers were observed on the electrospun PS reference fibers (Figure S5C, Supporting Information). In contrast, mesostructured fibers were found with the patchy PS$_{core}$/SED*i*PA fibers (Figure S5D, Supporting Information). In this sample, many short supramolecular nanofibers

were predominantly formed on the polymer fibers' surface. This confirms that the patchy worm-like SED*i*PA micelles initiate the self-assembly and promote the fixation of the supramolecular nanofibers on the supporting PS fibers.

To transfer and make use of our concept, we used a free-standing, electrospun patchy PS_{core}/SED*i*PA nonwoven in order to create a 3D hierarchically mesostructured nonwoven of sufficient size and stability. Figure S6 in the Supporting Information shows an optical image of the free-standing nonwoven as well as a SEM image. In a similar manner as described above, hierarchically mesostructured nonwovens were prepared by immersing the patchy PS_{core}/SED*i*PA nonwovens in an *i*Pr-BTA solution and subsequent drying at ambient conditions. Representative morphologies of hierarchically mesostructured nonwovens when a 0.10 wt% or a 0.50 wt% *i*Pr-BTA solution in isopropanol was used for the immersion process are depicted in **Figure 3**. Both nonwoven composites show short supramolecular nanofibers, which are either off-standing or on top of the PS_{core}/SED*i*PA fibers, resembling a barbed wire-like morphology. The higher *i*Pr-BTA concentration of the immersion solution leads to supramolecular nanofibers with a predominantly increased fiber length (Figure 3B). We note that much shorter supramolecular nanofibers were found within the hierarchically mesostructured nonwovens compared to the supramolecular nanofibers, which were formed by the molecular self-assembly of neat *i*Pr-BTA upon solvent evaporation for the same concentrations (Figure S4, Supporting Information). Moreover, electrospun nonwovens with a higher fiber density have also an influence on the morphology depending on the concentration of *i*Pr-BTA. For instance, the use of the 0.10 wt% solution resulted in a similar barbed wire-like morphology (Figure S7A, Supporting Information). The immersion of such a dense nonwoven into a 0.50 wt% *i*Pr-BTA solution led to a mesostructured nonwoven with a significantly denser network of supramolecular nanofibers (Figure S7B, Supporting Information). This might be attributed to the higher density of the polymer fibers within the electrospun nonwoven together with the complex drying process in nonwovens.

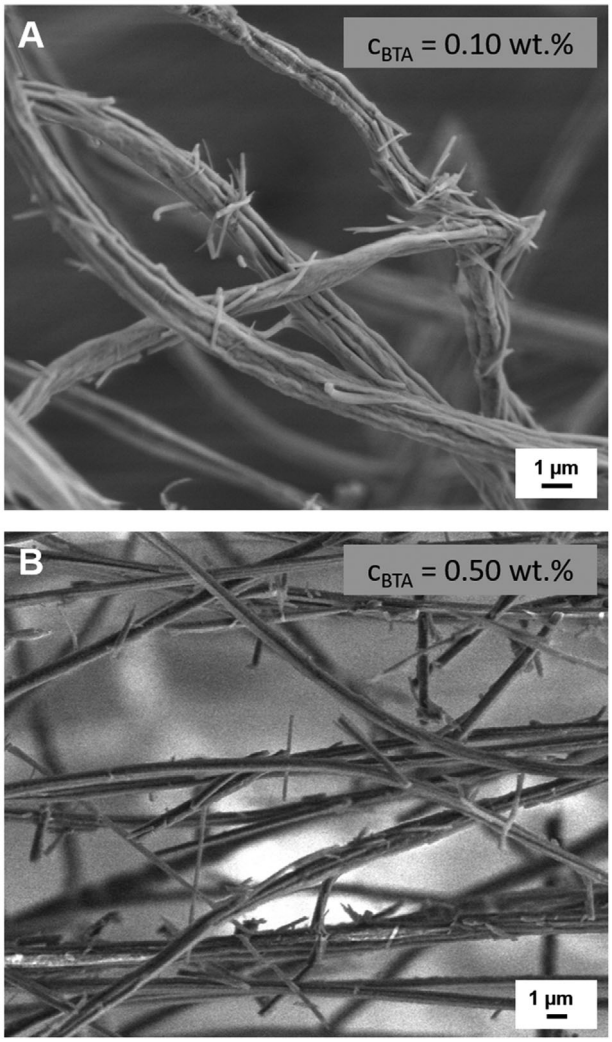

Figure 3. SEM images of hierarchically mesostructured nonwovens with functional supramolecular *i*Pr-BTA nanofibers. The mesostructured nonwovens were prepared by immersion of electrospun patchy PS_{core}/SED*i*PA nonwovens in isopropanol solutions with a *i*Pr-BTA concentration of A) 0.10 wt% and B) 0.50 wt% and subsequent drying at ambient conditions.

2.3. Functionalization of Hierarchically Mesostructured Nonwovens with Palladium Nanoparticles

Fibrous supramolecular composites featuring a high surface area with distinct functional groups on the surface are highly suitable for metal nanoparticle capture from solution,[4,43] rendering our mesostructured nonwovens with a barbed wire-like morphology and functional *N,N*-diisopropylaminoethyl groups promising candidates.

To demonstrate the proof-of-concept, we have used palladium nanoparticles (PdNPs) which can be conveniently synthesized and dispersed in aqueous media (see the Experimental Section). The size distribution of the PdNPs was investigated by transmission electron microscopy (TEM) and evaluation of at least 150 particles yielded an average particle diameter of $d_{TEM} = 2.7 \pm 0.4$ nm (Figure S8, Supporting Information).

For immobilization of the PdNPs a functional mesostructured nonwoven, prepared as described before by immersing a patchy PS_{core}/SED*i*PA nonwoven in a 0.50 wt% *i*Pr-BTA solution, was employed. PdNPs were immobilized by dipping the mesostructured nonwoven into the PdNP dispersion for 3 h at room temperature and subsequent drying at ambient conditions. Notably, after dipping of the hierarchical mesostructured nonwoven into the aqueous nanoparticle dispersion and drying, the shape of the nonwoven and the morphology is largely maintained under these conditions (Figure S9, Supporting Information). SEM images reveal no significant changes with respect to the PS_{core}/SED*i*PA nonwoven shape in general after immersion in *i*Pr-BTA isopropanol solution (Figure S9A, Supporting Information) or into the aqueous PdNP dispersion (Figure S9B, Supporting Information). The appearance of the supramolecular nanofibers of the mesostructured nonwoven also do not change after the immersion process. The SEM images show that PdNPs or agglomerates can be detected since they appear bright as they have a higher scattering intensity than the polymer fibers and the supramolecular fibers. To provide evidence on the particle size and particle

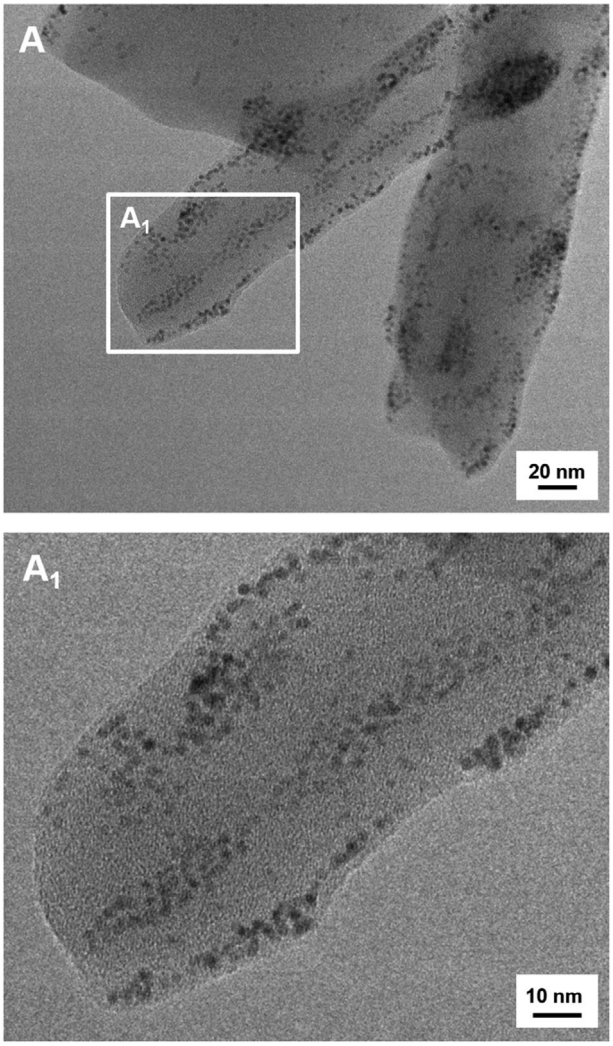

Figure 4. A) TEM images and magnification A_1) of a supramolecular *i*Pr-BTA nanofiber with immobilized palladium nanoparticles (PdNPs). For TEM sample preparation, a PdNP-loaded, hierarchically mesostructured nonwoven was mechanically broken.

distribution of single PdNPs on the BTA surface, TEM measurements of the functionalized nonwoven were conducted. As shown in **Figure 4**, only single PdNPs were deposited on the supramolecular short BTA nanofibers. By evaluation of 50 particles, we found a PdNP diameter of $d_{TEM} = 2.7 \pm 0.4$ nm. This particle size corresponds well to the size of the synthesized PdNPs, indicating a predominantly single, nonagglomerated nanoparticle uptake from solution rather than during the drying process.

These findings demonstrate that the fiber composites with a barbed wire-like morphology comprising functional supramolecular nanofibers are highly stable in aqueous media and allow for the efficient immobilization of individual PdNPs without agglomeration.

3. Conclusion

We have demonstrated the preparation of functional, hierarchically mesostructured nonwovens with a barbed wire-like fiber morphology which are suitable to immobilize metal nanoparticles. These mesostructured nonwovens were realized by combining electrospun polystyrene fibers, decorated with patchy worm-like micelles, with supramolecular nanofibers based on a 1,3,5-benzoltricarboxamide with functional peripheral *N,N*-diisopropylaminoethyl groups (*i*Pr-BTA). Mediation and initiation of the supramolecular nanofiber growth from the surface of the supporting electrospun polymer fibers was accomplished by the functional patches on top of the electrospun fibers, featuring on one hand pendant *N,N*-diisopropylaminoethyl groups matching the peripheral groups of *i*Pr-BTA. On the other hand, the polystyrene patches of the worm-like micelles ensure a proper fixation of the supramolecular *i*Pr-BTA nanofibers on the supporting polystyrene fibers. These hierarchically mesostructured nonwovens were shown to be highly suitable for the immobilization of palladium nanoparticles from aqueous media which are deposited on the surface of the functional supramolecular nanofibers. We anticipate that the combination of a complex mesoscale morphology with a specific functionalization of such nonwovens are attractive candidates to be used in filtration and separation and for heterogenous catalysis with metal nanoparticles.

4. Experimental Section

Materials: *N,N*-Diisopropylethylenediamine (ABCR), *n*-butyllithium (2.5 mol L^{-1} in hexane, Acros Organics), *N,N*-dimethylformamide (DMF, 99%, Acros Organics), tetrahydrofuran (THF, ≥ 99.9%, VWR), sodium tetrachloropalladate(II) (Na_2PdCl_4, ≈36% Pd, Acros Organics), 4-dimethylaminopyridine (DMAP, ReagentPlus, ≥99%, Sigma-Aldrich), sodium borohydride ($NaBH_4$, ≥ 96%, Fluka) were used as received. Isopropanol and pentane (technical grade) were distilled prior to use. THF used for the post-polymerization amidation was dried by successive distillation over calcium hydride and potassium prior to use. Deionized water with a conductivity of 18.2 MΩ cm was obtained by filtration through a Millipore Milli-Q Plus system (QPAK two purification cartridge). Polystyrene (PS) with a $M_n = 1.8 \times 10^6$ g mol^{-1} and $Đ = 1.08$ was prepared according to standard anionic polymerization procedures.

Synthesis and Preparation: N^1,N^3,N^5-tris[2-(diisopropylamino)-ethyl]-1,3,5-benzenetricarboxamide (*i*Pr-BTA) was synthesized in a two-step reaction route accordingly to our previous work.[33] Briefly, 7.17 g (0.028 mol) of trimesic acid trimethyl ester were dispersed in 25.0 mL (20.5 g, 0.142 mol) of *N,N*-diisopropylethylenediamine under argon atmosphere. The mixture was heated to 125 °C, stirred for 17 h and subsequently allowed to cool down to room temperature. The crude product was boiled two times in around 400 mL acetic acid ethyl ester and filtered. The product was dried under high vacuum overnight resulting in 12.2 g (72%) of *i*Pr-BTA as a white powder. ^{1}H NMR (300 MHz, $CDCl_3$, δ): 1.06 (d, 36H), 2.71 (t, 6H), 3.07 (m, 6H), 3.45 (quartett, 6H), 7.24 (t(br), 3H), 8.41 (s, 3H) ppm; ^{13}C NMR (75 MHz, $CDCl_3$, δ): 20.9, 38.5, 42.8, 47.8, 127.8, 135.3, 165.2 ppm; EIMS m/z (%): 588 (7) [M^+], 115 (96), 114 (100), 72 (97), 43 (35); MALDI-ToF MS m/z 589 [M•+H]$^+$; Anal. calcd. for $C_{33}H_{60}N_6O_3$: C 67.3, H 10.3, N 14.3; found: C 67.3, H 9.8, N 14.0%.

The polystyrene-*block*-polyethylene-*block*-poly(*N,N*-diisopropylaminoethyl methacrylamide) triblock terpolymer ($S_{28}E_{15}DiPA_{58}^{156}$, subscripts denote the mass fraction of the corresponding block in wt% and the superscript gives the overall number average molecular weight (M_n) in kg mol^{-1}) was prepared by post-polymerization functionalization of the poly(methyl methacrylate) block of the respective polystyrene-*block*-polyethylene-*block*-poly(methyl methacrylate) ($S_{40}E_{21}M_{39}^{108}$) triblock terpolymer precursor, according to our previous work.[29] In brief, *N,N*-diisopropylethylenediamine was first activated by deprotonation of the primary amino group with *n*-butyllithium in THF at −78 °C followed by heating to room temperature. Subsequently,

the activated amine solution (twofold excess of amine with respect to methyl ester units) was added to a THF solution of $S_{40}E_{21}M_{39}^{108}$ (c = 10 g L^{-1}) at 40 °C allowing the reaction to proceed for 24 h. The amidated polymer ($S_{28}E_{15}DiPA_{58}^{156}$) was isolated by precipitation from pentane. The employed $S_{40}E_{21}M_{39}^{108}$ triblock terpolymer was synthesized by a combination of sequential living anionic polymerization and catalytic hydrogenation, as described elsewhere.[42,44]

Patchy, worm-like SED*i*PA micelles were prepared by crystallization-driven self-assembly in THF. To this end, the $S_{28}E_{15}DiPA_{58}^{156}$ triblock terpolymer was first molecularly dissolved in THF (c = 10 g L^{-1}) at 65 °C for 30 min using a temperature-controllable shaker unit (HCL-MKR 13, Ditabis), followed by cooling to the crystallization temperature of the polyethylene (PE) middle block (T_c = 15 °C) to induce PE crystallization. The self-assembly process was allowed to proceed for 24 h at 200 rpm resulting in a dispersion of patchy worm-like micelles (average length: l = 260 ± 100 nm; patch sizes: 12 ± 2 nm (PS), 10 ± 3 nm (PD*i*PA); determined by TEM image analysis of at least 100 micelles by the software *ImageJ*.[45]

PS fibers and nonwovens decorated with patchy, worm-like SED*i*PA micelles were produced by coaxial electrospinning, in a similar manner as described previously.[30] A 7 wt% PS (M_n = 1.8 × 10^6 g mol^{-1}) solution in DMF was used as core to yield the supporting PS fiber, and a dispersion of patchy worm-like SED*i*PA micelles at a concentration of c = 10 g L^{-1} in THF was employed as shell (Figure S2, Supporting Information). Thin layers of patchy PS_{core}/SED*i*PA fibers were spun on aluminum foil placed at a distance of 20 cm from the coaxial needle (COAX_2DISP sealed coaxial needles, LINARI NanoTech, d_{core} = 0.51 mm and d_{shell} = 1.37 mm) at a temperature of 20.8 °C and a relative humidity of around 30% (feed rates: 1.2 mL h^{-1} (PS solution, core), 1.0 mL h^{-1} (micelle dispersion, shell)). Corresponding free-standing nonwovens were spun on a rotating disk collector (D = 20 cm, 800 rpm) placed at a distance of 5 cm of the coaxial needle. For electrospinning, a voltage of 11.4 kV at the needle and −1.0 kV at the collector were applied. Neat PS fibers were prepared as reference material in the same manner but without using the micellar dispersions.

Hierarchically mesostructured fibers/nonwovens were prepared by immersion of the electrospun PS_{core}/SED*i*PA fibers/nonwovens in a BTA solution in isopropanol at a concentration of c = 0.10 or 0.50 wt%. The immersion time was varied from 30 s to 5 h to 12 h at room temperature. We noted that the immersion time does not play a significant role on the resulting morphology because at already short immersion times the nonwoven is completely filled with the solution. Subsequently, the solvent was evaporated at ambient conditions by fixing the nonwoven in a vertical position.

DMAP-stabilized palladium nanoparticles (PdNPs) were synthesized according to literature procedure.[46] Therefore, 40.0 mg Na_2PdCl_4 were dissolved in 3.23 g deionized water. 9.65 g of a 75.8 × 10^{-3} M aqueous DMAP solution was added and stirred for 20 min. Afterwards, 1.1 mL of a 1% w/v aqueous $NaBH_4$ solution was added.

PdNPs were immobilized by immersion of a hierarchical mesostructured nonwoven in an aqueous dispersion of PdNPs (c = 0.0258 g L^{-1}) for 3 h at room temperature and subsequent solvent evaporation in a vertical position at ambient conditions.

Molecular Characterization: ^{1}H NMR (300 MHz) and ^{13}C NMR (75 MHz) measurements were carried out on a Bruker Avance AC 300 spectrometer at room temperature. Mass spectra were recorded on a Finnigan MAT 8500 spectrometer (EI, 70 eV) using direct injection mode. Elemental analysis (C, H, N) was carried out with a Unicube from Elementar Analysen-Systeme with sulfanilamide as standard. The theoretical amount of all elements was calculated using Chemicalize. Values are given in wt%. Matrix-assisted laser desorption/ionization time-of-flight mass spectroscopy (MALDI-ToF MS) measurements were performed using a Bruker AutoFlex Max mass spectrometer equipped with a Smartbeam II laser. The analyte was embedded in the matrix material trans-2-[3-(4-tert-butylphenyl)-2-methyl-2-propenylidene]malononitrile (DCTB) in the matrix:analyte mass ratio 10:1. FT-IR spectra was recorded with a Perkin-Elmer Spectrum 100 FT-IR spectrometer using the attenuated total reflectance unit.

Methods: Temperature-dependent transmittance of BTA solutions were determined at a wavelength of λ = 645 nm using the crystallization system Crystal16 (Technobis Crystallization Systems). Solutions or dispersions of the BTA in isopropanol were prepared in a concentration range between 0.25 and 4.25 wt% in 0.25 wt% steps at room temperature and stirred at 600 rpm with a stirring bar. The samples were heated to 70 °C with 10 K min^{-1} and hold isothermally for 30 min within the crystallization system. After that, the transmittance at λ = 645 nm of the samples was recorded for three cycles from 70 to −5 °C. Each cycle comprises a cooling step with 0.1 K min^{-1}, an isothermal at −5 °C for 10 min, a subsequent heating step with a rate of 0.1 K min^{-1}, and an isothermal at 70 °C for 10 min. The cloud and clearing points were determined at a transmission of 50% upon cooling and heating, respectively. The given cloud and clearing points, as depicted in Figure 2B, are the mean values from three cooling and heating cycles, respectively.

SEM measurements were conducted with a FEI Quanta FEG 250 scanning electron microscope (Thermo Fisher Scientific) equipped with a field emission gun. For SEM, all samples were used without applying sputter coating. For Figure S5A,B,D (Supporting Information) measurements were conducted in the beam deceleration mode under high vacuum at an acceleration voltage of 6 kV. Here, an additional negative voltage of −4 kV was applied to the stage to decelerate the primary electrons to 2 kV. The electrons interacting with the sample were accelerated towards the concentric back scattered (CBS) detector. The samples measured in the beam deceleration mode were placed on the sample table and fixed with a conductive tape. All other SEM images were recorded in the low vacuum mode (water pressure of 40 Pa in the sample chamber) with an acceleration voltage of 3 or 5 kV with a large-field (gaseous secondary electron) detector for topographical details or CBS detector to visualize the PdNPs. The samples measured in the low vacuum mode were mounted on a sample holder using a double-sided adhesive graphite pad.

TEM measurements were performed with a JEOL JEM-2200FS equipped with a Gatan OneView CMOS camera using the Digital Micrograph Software. For the investigation of the size distribution of the nanoparticles, a small drop of the suspension with the PdNPs was placed onto a carbon-coated copper grid (S160, Plano EM, Germany) and excess solution was removed by a filter paper. For the investigation of the PdNPs distribution on the supramolecular fibers, a lacey carbon-coated copper grid (S166, Plano EM, Germany) was wiped over the surface of the functional, hierarchically mesostructured nonwoven to prepare the TEM sample. All specimens were investigated at room temperature using the bright-field mode at an acceleration voltage of 200 kV.

Supporting Information

Supporting Information is available from the Wiley Online Library or from the author.

Acknowledgements

This work was supported by the German Research Foundation (DFG) in the framework of the Collaborative Research Centre SFB840, projects A2 and B8. The authors thank Prof. Andreas Greiner for helpful discussions and his support with the coaxial electrospinning facility. The authors thank Sandra Ganzleben (Macromolecular Chemistry I, University of Bayreuth) for the support with the synthesis. The authors also thank Andreas Erhardt (Macromolecular Chemistry I, University of Bayreuth) for conducting the MALDI-ToF MS measurement. Hannah Kurz (Inorganic Chemistry IV, University of Bayreuth) is acknowledged for carrying out the elemental analysis. The authors acknowledge the support of the Keylabs Electron and Optical Microscopy and Synthesis and Molecular Characterization of the Bavarian Polymer Institute at the University of Bayreuth. A.F. thanks the Elite Study Program *Macromolecular Science* within the Elite Network of Bavaria (ENB) for support.

Open access funding enabled and organized by Projekt DEAL.

Conflict of Interest

The authors declare no conflict of interest.

Data Availability Statement

The data that support the findings of this study are available from the corresponding author upon reasonable request.

Keywords

1,3,5-benzenetricarboxamides, mesostructured nonwovens, molecular and crystallization-driven self-assembly, patchy worm-like micelles, supramolecular nanofibers

Received: January 21, 2022
Revised: March 14, 2022
Published online: April 4, 2022

[1] L. De Sio, B. Ding, M. Focsan, K. Kogermann, P. Pascoal-Faria, F. Petronela, G. Mitchell, E. Zussman, F. Pierini, *Chemistry* **2021**, *27*, 6112.
[2] M. Hu, Y. Wang, Z. Yan, G. Zhao, Y. Zhao, L. Xia, B. Cheng, Y. Di, X. Zhuang, *J. Mater. Chem. A* **2021**, *9*, 14093.
[3] S. Zhang, H. Liu, N. Tang, S. Zhou, J. Yu, B. Ding, *Adv. Mater.* **2020**, *32*, 2002361.
[4] M. Drummer, C. Liang, K. Kreger, S. Rosenfeldt, A. Greiner, H.-W. Schmidt, *ACS Appl. Mater. Interfaces* **2021**, *13*, 34818.
[5] A. Anstey, E. Chang, E. S. Kim, A. Rizvi, A. R. Kakroodi, C. B. Park, P. C. Lee, *Prog. Polym. Sci.* **2021**, *113*, 101346.
[6] X. Zhang, Y. Lu, *Polym. Rev.* **2014**, *54*, 677.
[7] Z.-M. Zhang, Y.-S. Duan, Q. Xu, B. Zhang, *J. Eng. Fibers Fabr.* **2019**, *14*, 155892501986751.
[8] B. Atıcı, C. H. Ünlü, M. Yanilmaz, *Polym. Rev.* **2021**, *62*, 1.
[9] D. Li, Y. Xia, *Adv. Mater.* **2004**, *16*, 1151.
[10] A. Greiner, J. H. Wendorff, *Angew. Chem., Int. Ed.* **2007**, *46*, 5670.
[11] S. Agarwal, A. Greiner, J. H. Wendorff, *Adv. Funct. Mater.* **2009**, *19*, 2863.
[12] S. Jung, J. Kim, *Polymers* **2020**, *12*, 1714.
[13] Y. Li, X. Yin, J. Yu, B. Ding, *Compos. Commun.* **2019**, *15*, 6.
[14] S. Zhang, H. Liu, X. Yin, J. Yu, B. Ding, *ACS Appl. Mater. Interfaces* **2016**, *8*, 8086.
[15] S. Zhang, N. Tang, L. Cao, X. Yin, J. Yu, B. Ding, *ACS Appl. Mater. Interfaces* **2016**, *8*, 29062.
[16] Z. Wang, Z. Pan, *Appl. Surf. Sci.* **2015**, *356*, 1168.
[17] Z. Su, J. Ding, G. Wei, *RSC Adv.* **2014**, *4*, 52598.
[18] H. Misslitz, K. Kreger, H.-W. Schmidt, *Small* **2013**, *9*, 2053.
[19] D. Weiss, D. Skrybeck, H. Misslitz, D. Nardini, A. Kern, K. Kreger, H.-W. Schmidt, *ACS Appl. Mater. Interfaces* **2016**, *8*, 14885.
[20] Y. Wang, G. Chao, X. Li, F. Dong, X. Zhuang, L. Shi, B. Cheng, X. Xu, *Soft Matter* **2018**, *14*, 8879.
[21] M. Burgard, D. Weiss, K. Kreger, H. Schmalz, S. Agarwal, H.-W. Schmidt, A. Greiner, *Adv. Funct. Mater.* **2019**, *29*, 1903166.
[22] A. M. Oliver, J. Gwyther, C. E. Boott, S. Davis, S. Pearce, I. Manners, *J. Am. Chem. Soc.* **2018**, *140*, 18104.
[23] S. Ganda, M. H. Stenzel, *Prog. Polym. Sci.* **2020**, *101*, 101195.
[24] L. MacFarlane, C. Zhao, J. Cai, H. Qiu, I. Manners, *Chem. Sci.* **2021**, *12*, 4661.
[25] C. Hils, I. Manners, J. Schöbel, H. Schmalz, *Polymers* **2021**, *13*, 1481.
[26] A. Frank, C. Hils, M. Weber, K. Kreger, H. Schmalz, H.-W. Schmidt, *Angew. Chem., Int. Ed.* **2021**, *60*, 21767.
[27] S. Cantekin, T. F. A. de Greef, A. R. A. Palmans, *Chem. Soc. Rev.* **2012**, *41*, 6125.
[28] J. Schöbel, M. Burgard, C. Hils, R. Dersch, M. Dulle, K. Volk, M. Karg, A. Greiner, H. Schmalz, *Angew. Chem., Int. Ed.* **2017**, *56*, 405.
[29] J. Schöbel, C. Hils, A. Weckwerth, M. Schlenk, C. Bojer, M. C. A. Stuart, J. Breu, S. Förster, A. Greiner, M. Karg, H. Schmalz, *Nanoscale* **2018**, *10*, 18257.
[30] C. Hils, M. Dulle, G. Sitaru, S. Gekle, J. Schöbel, A. Frank, M. Drechsler, A. Greiner, H. Schmalz, *Nanoscale Adv.* **2020**, *2*, 438.
[31] D. Besold, S. Risse, Y. Lu, J. Dzubiella, M. Ballauff, *Ind. Eng. Chem. Res.* **2021**, *60*, 3922.
[32] P. Hervés, M. Pérez-Lorenzo, L. M. Liz-Marzán, J. Dzubiella, Y. Lu, M. Ballauff, *Chem. Soc. Rev.* **2012**, *41*, 5577.
[33] A. Frank, A. Bernet, K. Kreger, H.-W. Schmidt, *Soft Matter* **2020**, *16*, 4564.
[34] C. Hils, E. Fuchs, F. Eger, J. Schöbel, H. Schmalz, *Chem. – Eur. J.* **2020**, *26*, 5611.
[35] Bo Pang, Y. Yu, W. Zhang, *Macromol. Rapid Commun.* **2021**, *42*, 2100504.
[36] T. Thavanesan, C. Herbert, F. A. Plamper, *Langmuir* **2014**, *30*, 5609.
[37] P. J. M. Stals, M. M. J. Smulders, R. Martín-Rapún, A. R. A. Palmans, E. W. Meijer, *Chem. – Eur. J.* **2009**, *15*, 2071.
[38] X.-J. Kuang, A. Wajahat, W.-T. Gong, M. K. Dhinakaran, X.-H. Li, G.-L. Ning, *Soft Matter* **2017**, *13*, 4074.
[39] A. Paikar, A. Pramanik, D. Haldar, *RSC Adv.* **2015**, *5*, 31845.
[40] V. Nagarajan, V. R. Pedireddi, *Cryst. Growth Des.* **2014**, *14*, 1895.
[41] S. Kumar, S. Bera, S. K. Nandi, D. Haldar, *Soft Matter* **2021**, *17*, 113.
[42] J. Schmelz, M. Karg, T. Hellweg, H. Schmalz, *ACS Nano* **2011**, *5*, 9523.
[43] E. Krieg, H. Weissman, E. Shirman, E. Shimoni, B. Rybtchinski, *Nat. Nanotechnol.* **2011**, *6*, 141.
[44] H. Ruckdäschel, J. K. W. Sandler, V. Altstädt, C. Rettig, H. Schmalz, V. Abetz, A. H. E. Müller, *Polymer* **2006**, *47*, 2772.
[45] W. S. Rasband, *U. S. ImageJ*, National Institutes of Health, Bethesda, Maryland, USA, https://imagej.nih.gov/ij/ (accessed: 2022).
[46] K. A. Flanagan, J. A. Sullivan, H. Müeller-Bunz, *Langmuir* **2007**, *23*, 12508.

